AUT Journal of Mechanical Engineering

AUT J. Mech. Eng., 1(2) (2017) 119-130
DOI: 10.22060/mej.2017.12928.5472

Numerical Analysis of Critical Heat Flux Phenomenon in a Nuclear Power Plant Core Channel in the Presence of Mixing Vanes

A. Rabiee*, L. Moradi, A. Atf

School of Mechanical Engineering, Shiraz University, Shiraz, Iran

ABSTRACT: The necessity and importance of a high heat removal potential in various areas particularly in nuclear applications are in a direct relationship with the excessively applied heat flux level. One way to increase the heat transfer performance and subsequently enhance the threshold of the critical heat flux is to employ spacer grids accompanied by mixing vanes. In this study, the effect of the spacers with mixing vanes on the critical heat flux characteristics in the dryout condition has been numerically investigated employing the benefits of the Eulerian-Eulerian framework. In the current research, several vane angles, including vane with 0, 15 and 25 degrees in comparison with the effect of the bare spacer without any mixing vanes on the flow characteristics were examined. It was shown that the existence of the spacer alone, delays the temperature jump under critical heat flux conditions. It was also concluded that increasing the angle of the mixing vanes, further improves the heat transfer performance of the system by postponing the sudden temperature jump occurring in the channel; however, the presence of the spacers and vanes in the flow field imposes an increase of the pressure drop due to the constriction on the coolant flow area.

Review History:

Received: 24 May 2017
Revised: 24 June 2017
Accepted: 16 July 2017
Available Online: 21 October 2017

Keywords:

Boiling
Critical heat flux
Mixing vane
Spacer grid

1- Introduction

Spacer grids in the nuclear fuel rod assembly provide a mechanical support which preserves a constant distance between the fuel rods and also prevents the fuel rod damage from flow-induced vibrations. Mixing vanes attached to the spacer grids produce a swirling flow in the subchannel and consequently increase the overall heat transfer performance as an essential design factor. Enhancing the critical heat flux (CHF) threshold of boiling systems which would lead to an improved thermal efficiency and reduced operational costs, has been the main goal of researchers and scientists in various areas for several decades. Mixing vane installation is an effective technique to reach this goal. The present article covers the evaluation of the mixing vanes presence on the boiling flow field accompanied by a critical heat flux using computational fluid dynamics. The activities performed by researchers in this area are mentioned in the following.

Shin et al. [1] experimentally studied the effect of angles and positions of mixing vanes on the critical heat flux in a 2×2 rod bundle with working fluid R-134a. In the CHF experiment, various mixing vane angles between 20-40 degrees have been studied. The CHF enhancement ratio (CER) had the greatest value at 30 degrees and the maximum critical heat flux enhancement was about 19%. A CHF experiment on the position of the mixing vane also showed that by weakening the swirl flow as one of the consequences of increasing distance between grid and CHF location, CER would be decreased.

Lee et al. [2] assessed the thermal-hydraulic characteristics of hybrid mixing vanes in a 17×17 nuclear rod bundle. Different types of mixing vanes were investigated and compared with each other and it was found that the hybrid mixing vanes have a greater influence on the flow characteristics such as the secondary intensity and also Nusselt number. Therefore, lower amounts of wall temperature would be achieved which would enhance the safety margins of the operating conditions of the system. Krepper et al. [3] investigated the subcooled flow boiling in a fuel assembly by employing the benefits of computational fluid dynamics code, CFX software. The model is applied to consider the occurrences inside a hot channel of an assembly in the presence of the mixing vanes. The numerical results were in a good agreement with the available experimental data, indicating that the used models had the capability to inspect the boiling flow and phase transition. Navarro et al. [4] numerically assessed flow field of a 5×5 PWR rod bundle accompanied by mixing vane spacer using the CFX commercial software. In order to simulate the flow field inside the channel, the computational domain was separated in seven subdomains. In the next step, the numerical results of the numerical simulation were compared with the available experimental data and a good agreement was achieved. Moreover, the obtained numerical results predicted the flow characteristics more precisely with respect to the previous models. Shin et al. [5] performed a study on a 2×3 rod bundle with mixing vane experimentally and numerically. The experiment was conducted under various conditions in such a way that the CHF enhancement was the largest at the operating conditions with 1400 kg/m2 s mass flux and 15 bar pressure. Furthermore, different mixing vane shapes were examined and it was revealed that the swirl vane type was more efficient with low pressure and mass flux conditions while the hybrid type performed better near the operating conditions of a pressurized water reactor (PWR). The presence of mixing vanes caused a lateral flow among the channels and as result, the void fraction distribution near the heated wall was reduced which gave rise to the CHF enhancement. Damsohn et al. [6] experimentally examined

Corresponding author, E-mail: rabiee@shirazu.ac.ir

the effect of spacer grids on the dryout phenomenon in nuclear rod bundles representing a boiling water reactor subchannels. In the current study, air and water were considered to simulate the dryout conditions in the channel. The effect of the presence of the spacers with various shapes and also different superficial velocities on the existing thin liquid film on the heated wall was investigated. The results illustrated that the liquid film did not show a specific trend, such that it was thinned and thickened at different locations downstream of the spacer grids. Jun et al. [7] carried out a thermal hydraulic evaluation and safety analysis of a system by the TASS/SMR-S code. In the current research, the employed heat transfer model in TASS/SMR-S code was validated by the available experimental data of Bennett's heated tube tests and THTF (thermal hydraulic test facility) [8]. The critical heat flux point and also the wall temperature along the channel were reported from the outcomes of the TASS/SMR-S code. Jayanti et al. [9] investigated the effect of spacer grids on flow and heat transfer in rod bundles. The simulation was carried out by using the computational fluid dynamics (CFD) within a Eulerian-Lagrangian framework for the calculation and consideration of various flow regimes occurring in the corresponding channel. It was shown that the single-phase convective heat transfer coefficient was increased up to 40 percent in the vicinity of the spacer grid, leading to a wall temperature reduction. In addition, some calculations regarding the droplet trajectory illustrated that the rate of droplet deposition is significantly increased in the spacer region. Nazififard et al. [10] evaluated the thermal-hydraulic characteristics of an advanced pressurized water reactor with 3×3 rod bundle array. The effect of the spacer grid and standard split-type vane was numerically investigated by the use of ANSYS FLUENT software, and it was found that the Nusselt number gradually decreased downstream of the grid spacers and mixing vane and approached to a fully developed value downstream of the spacer grids. Zhu et al. [11] investigated the effect of the spacer grid on the heat transfer of supercritical water flows in a rod bundle using commercial CFD code STAR CCM6.04 . In their research, they tried to inspect the thermal-hydraulic aspect of the subchannel by considering the standard spacer grid and the spacer grid with split-vanes. It was concluded that the heat transfer performance of the channel was impressively improved within and also in the downstream of the spacer grid as a result of the reduced flow area of the channel. Seo et al. [12] experimentally and numerically studied the performance of the rotating mixing vanes in increasing the critical heat flux enhancement. A swirl generating device called the rotational vane was employed for the heat transfer characteristics enhancement purposes. The created centrifugal force as a result of employment of the moving rotating vanes would lead to a remarkable increase of the critical heat flux level. The experiments were carried out in both horizontal and vertical channels with different mixing vane shapes. Among all of the various mixing vane shapes, the moving rotational vane produced more swirl and secondary flows indicating that the best heat transfer behavior would be achieved in this circumstance. Mimouni et al. [13] predicted critical heat flux in boiling flow using computational multi-fluid dynamics. A new mechanistic model in a computational multi-fluid dynamics was suggested with the intention of simulating the wall temperature sudden jump and also the boiling crisis conditions. The achieved results were compared with the 150 tests and a relatively good agreement between the results was evidenced. Chen et al. [14] investigated the thermal-hydraulic performance of a 5×5 nuclear rod bundle with and without spacer grid. For the purpose of simulating the complicated flow in the rod bundle, various turbulence models were applied in the available CFD code. The obtained numerical results of the temperature distribution at the outlet section were compared with the experimental data as well. It was concluded that the secondary flow induced by the presence of the spacer grids has a noticeable influence on the thermal-hydraulic behavior of the system. Zhao et al. [15] carried out an experiment inspecting the heat transfer of water flowing upward in vertical annuli with spacers at high pressure conditions. The results suggest that the heat transfer coefficient would be significantly improved by the effect of the spacer on the flow field in the annuli. In addition, a correlation was proposed to involve the heat transfer improvement effects as a result of the spacers at supercritical pressure condition.

Based on the available data in the open literature, the effect of spacer grids accompanied by the existence of mixing vanes has been extensively studied especially in boiling flow regimes. However, there are a few limited studies that present the effect of mixing vanes on postponing the dryout phenomenon when the critical heat flux conditions have been reached. Moreover, most of these studies have been performed experimentally and a minority of them are accomplished by employing computational fluid dynamics and a detailed study of the flow situation has not yet been reported. Therefore, in this study, the effect of the presence of the spacers accompanied by mixing vanes on the critical heat flux characteristics in the dryout phenomenon has been investigated numerically by employing the Eulerian-Eulerian framework for each phase. A detailed description of the current simulation algorithm, including wall heat flux partitioning, turbulence, heat, and mass transfer models is demonstrated in the following section.

2- Numerical Simulation of Boiling Flow Field

In the present study, the Reynolds averaged Navier-Stokes equations have been solved in an Eulerian-Eulerian framework for the intention of modeling the boiling flow field and also some constitutional relations have been employed to describe the boiling phenomenon in equilibrium and non-equilibrium conditions. Wall boiling phenomenon is simulated using the mechanistic Rensselaer Polytechnic Institute (RPI) boiling model and the extended formulations for the departure from nucleate boiling. With the aim of considering the wall boiling regime transition from nucleate boiling to critical heat flux, topological functions have been used.

Itis noted that due to the existence of the high density ratio of the liquid and vapor phases particularly in the boiling flow field, employing a suitable strategy in order to achieve a converged solution is necessary. For this reason, SIMPLE algorithm method for coupling the pressure and velocity fields which leads to a more stable solution has been used. Furthermore, to discretize the diffusion and convective terms in the governing equations, first-order upwind scheme and linear interpolation method for computing the pressure particularly on the face of every computational cell have been employed. It should be mentioned that in addition to the selection of turbulence models such as k-w, using low

under-relaxation factors particularly at the first stages of the solution process, is suitable.
A comprehensive description of the models used in the available code (FLUENT) is identified in the following.

2- 1- Governing equations

The governing equations, including continuity, momentum and energy equations for each phase in a generalized arrangement besides the required relations are represented as:

$$\frac{\partial(\alpha_q\rho_q)}{\partial t}+\nabla.(\alpha_q\rho_q V_q)=\sum_{r=1}^{n}(\dot{m}_{rq}-\dot{m}_{qr})+s_q \tag{1}$$

where n is the number of phases in the system, $\dot{m}_{rq}$ denotes the mass transfer from r^{th} to q^{th} phase, $\dot{m}_{qr}$ is the mass transfer from q^{th} to r^{th} phase and s_q is the external mass source applied on the q^{th} phase [16].

$$\begin{aligned}&\frac{\partial(\alpha_q\rho_q V_q)}{\partial t}+\nabla.(\alpha_q\rho_q V_q V_q)=-\alpha_q\nabla p+\nabla.(\overline{\tau}_q)+\\&\alpha_q\rho_q B_f+\sum_{r=1}^{n}(F_{rq}^{D}+F_{rq}^{TD}+\dot{m}_{rq}V_{rq}-\dot{m}_{qr}V_{qr})+(F_q+F_q^{L}+F_q^{vm})\end{aligned} \tag{2}$$

Subscript "rq" indicates the interaction between the two phases, $\overline{\tau}_q$ is the stress-strain tensor in the q^{th} phase, $\boldsymbol{F}_{rq}^{TD}$ is the turbulent dispersed force, $\boldsymbol{V}_{rq}$ and $\boldsymbol{V}_{qr}$ are relative velocity vectors between the two phases and $\boldsymbol{F}_q$, $\boldsymbol{F}_q^{vm}$ and $\boldsymbol{F}_q^{L}$ are the external body, lift and virtual mass exchange forces, respectively [16].

$$\begin{aligned}&\frac{\partial(\alpha_q\rho_q H_q)}{\partial t}+\nabla.(\alpha_q\rho_q V_q H_q)=\overline{\tau}_q:\\&\nabla V_q+\alpha_q\frac{\partial p}{\partial t}-\nabla\dot{q}+S_{H,q}+\sum_{r=1}^{n}(\dot{q}_{rq}+\dot{m}_{rq}H_{rq}-\dot{m}_{qr}H_{qr})\end{aligned} \tag{3}$$

In Eq. (3), $\dot{q}_{rq}$ is the intensity of heat exchange between the phases, H_{rq} and H_{qr} are the inter-phase enthalpies [15].

2- 2- Turbulence modeling

Various multiphase turbulence models, including a range of 2-equation models, are offered in the available CFD code which are all usable in boiling flows. In Eq. (4), ϕ symbolizes turbulence scalar equations and consequently, the turbulence modeling equations can be represented by the following general equation:

$$\frac{\partial}{\partial t}(\alpha_q\rho_q\phi_q)+\nabla.(\alpha_q\rho_q V_q\phi_q)=\nabla.(\alpha_q\Gamma_{\phi,q}\nabla\phi_q)+\alpha_q S_{q,\phi} \tag{4}$$

In this equation, $\Gamma_{\phi,q}$, $S_{q,\phi}$ are the diffusion coefficient and the general source term which include production, dissipation and extra source terms stemming from turbulent-bubble interactions [16].
It is noted that k-ε turbulence model has been used in this research, preferably.

$$\begin{aligned}&\frac{\partial}{\partial t}(\alpha_q\rho_q k_q)+\nabla.(\alpha_q\rho_q V_q k_q)=\nabla.(\alpha_q(\mu_q+\frac{\mu_{t,q}}{\sigma_k})\nabla k_q)\\&+\alpha_q G_{k,q}-\alpha_q\rho_q\varepsilon_q+\alpha_q\rho_q\prod k_q\end{aligned} \tag{5}$$

$$\begin{aligned}&\frac{\partial}{\partial t}(\alpha_q\rho_q\varepsilon_q)+\nabla.(\alpha_q\rho_q V_q\varepsilon_q)=\nabla.(\alpha_q(\mu_q+\frac{\mu_{t,q}}{\sigma_k})\nabla\varepsilon_q)\\&+\alpha_q\frac{\varepsilon_q}{k_q}(C_{1\varepsilon}G_{k,q}-C_{2\varepsilon}\rho_q\varepsilon_q)+\alpha_q\rho_q\prod\varepsilon_q\end{aligned} \tag{6}$$

2- 3- Wall boiling models

RPI model developed by Kurul and Podowski [17] has been widely used as the modeling approach for the mechanistic prediction of boiling phenomenon. It is notable that in the current study, the applied total wall heat flux is divided into three parts, namely liquid phase convective heat flux (q_c), quenching heat flux (q_Q) and evaporation heat flux (q_E) as shown in Fig. 1.

$$\dot{q}_w=\dot{q}_c+\dot{q}_Q+\dot{q}_E \tag{7}$$

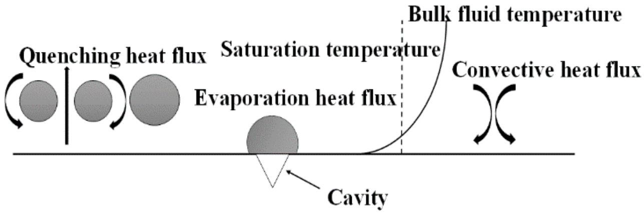

Fig. 1. A Schematic of different wall heat flux partitioning

2- 4- Liquid phase convective heat flux

$$\dot{q}_c=h_c(T_w-T_l)(1-A_b) \tag{8}$$

In Eq. (8), h_C is denoted as the liquid phase heat transfer coefficient, T_w and T_l are the wall and liquid temperature near the wall, respectively [16]. A_b is the area of influence which could be calculated in terms of the bubble departure diameter and the nucleate site density as follows:

$$A_b=\min(1,\eta\frac{\pi}{4}d_b^2N_w) \tag{9}$$

The empirical coefficient η can be calculated by the relation suggested by Valle and Kenning in 1985 [18]:

$$\eta=4.8\exp(-\frac{Ja}{80}) \tag{10}$$

And Ja is the subcooled Jacob number, which is defined as:

$$Ja=\frac{\rho_l C_{p,l}\Delta T_{sub}}{\rho_v H_{lv}} \tag{11}$$

2- 5- Quenching heat flux

Quenching heat flux partition is expressed as the following relation:

$$\dot{q}_Q=C_{wt}\frac{2k_l}{\sqrt{\frac{\pi\gamma_l}{f_{bw}}}}(T_w-T_{l,q})A_b \tag{12}$$

This term simulates the cyclic averaged transient energy transfer associated with liquid filling the wall vicinity after the bubble is detached from the wall with a period of $1/f_{bw}$ [16]. k_l, γ_l and f_{bw} are heat conductivity, diffusivity in the liquid phase and the frequency of bubble departure, respectively and C_{wt} is a constant coefficient, as well.

2- 6- Frequency of bubble departure

In this research, the frequency of bubble departure is computed based on the inertia controlled growth proposed by Cole [19]:

$$f_{bw} = \sqrt{\frac{4g(\rho_l - \rho_v)}{3\rho_l d_{bw}}} \tag{13}$$

2- 7- Evaporation heat flux

Evaporation heat flux is calculated by the following equation:

$$\dot{q}_E = \frac{\pi}{6} d_{bw}^3 f_{bw} N_w \rho_v H_{lv} \tag{14}$$

Where d_{bw} is the bubble departure diameter, N_w is the active nucleate site density, ρ_v is the vapor density, and H_{lv} is the latent heat of evaporation:

2- 8- Nucleation site density

In this study, the magnitude of nucleation site density is represented by the Lemmert-Chawla correlation in terms of the wall superheat [20]:

$$N_w = C^n (T_w - T_{sat}) \tag{15}$$

Here by default, C=15545.54 and n=1.805.

2- 9- Bubble departure diameter

Bubble departure diameter is modeled by the correlation proposed by Tolubinski [21]:

$$\mathrm{D}_w = \min(0.0014, 0.0006\exp(-\frac{\Delta T_w}{45})) \tag{16}$$

The function $f(\alpha_v)$ is in terms of the local vapor volume. It can be predicted by the relation offered by Ioilev et al. [22]:

$$\mathrm{f}(\alpha_v) = 1 - \mathrm{f}(\alpha_l) = \max(0, \min\left\{1, \frac{\alpha_v - \alpha_{v,1}}{\alpha_{v,2} - \alpha_{v,1}}\right\}) \tag{17}$$

2- 10- Modified RPI wall boiling model

In order to model the critical heat flux phenomenon, it is crucial to include the vapor temperature variation in the governing equations, while in the conventional RPI model, the vapor temperature is not calculated from solving the phase energy equation but fixed at the saturation temperature. In addition, thin liquid films along heated walls also need to be taken into account in the wall heat flux partitioning equation. For that reason, the wall heat partition is modified as follows [22]:

$$\dot{q}_w = (\dot{q}_c + \dot{q}_Q + \dot{q}_E + \dot{q}_F) f(\alpha_l) + (1 - \mathrm{f}(\alpha_l))\dot{q}_v + \dot{q}_G \tag{18}$$

The function $f(\alpha_v)$ is in terms of the local vapor volume. It can be predicted by the relation offered by Ioilev et al. [23, 24]:

$$\mathrm{f}(\alpha_v) = 1 - \mathrm{f}(\alpha_l) = \max(0, \min\left\{1, \frac{\alpha_v - \alpha_{v,1}}{\alpha_{v,2} - \alpha_{v,1}}\right\}) \tag{19}$$

It is noteworthy to mention that the flow regime transition occurs smoothly from a continuous liquid bubbly flow to churn and finally a continuous mist flow configuration in terms of single local flow quantity named the vapor volume fraction, α_v as follows[16, 22].

Bubbly flow topology: the vapor phase is dispersed in the continuous liquid in the form of bubbles ($\alpha_v \leq 0.3$).

Churn flow: this is an intermediate topology between the bubbly and mist flow topology, where $0.3 \leq \alpha_v \leq 0.7$

Mist flow topology: the liquid phase is dispersed in the continuous vapor in the form of droplets $\alpha_v \geq 0.7$.

Interfacial quantities such as interfacial area, drag, lift, turbulent drift force and heat transfer named ω, can be computed using the following general form:

$$\omega = (1 - \mathrm{f}(\alpha_v))\omega_{bubbly} + f(\alpha_v)\omega_{droplet} \tag{20}$$

Here ω_{bubbly} and $\omega_{droplet}$ are the interfacial quantities from the bubbly flow and mist flow, respectively [16].

2- 11- Interfacial transfer

In this study, the interfacial area, momentum transfer terms such as drag, lift, and turbulent quantities are determined as follows:

2- 11- 1- Interfacial area

The interfacial area is one of the important parameters for the momentum and heat transfer processes. The following relation is used in the current study:

$$A_i = \frac{6(1 - \alpha_d)\alpha_d}{D_d} \tag{21}$$

Here, subscript "d" represents a dispersed phase, which is the vapor phase in bubbly flows and the liquid phase in mist flows [16].

2- 11- 2- Interfacial momentum transfer

In boiling flow regimes, the most important interfacial momentum transfers are drag, lift and turbulent drift forces which are described in the subsequent sections.

2- 11- 3- Interfacial drag force

For dispersed bubbly and mist flows, the interfacial drag force has the general form:

$$F_{lv}^D = -F_{vl}^D = \frac{A_i}{8} \rho_c C_{lv}^D |V_l - V_v| (V_l - V_v) \tag{22}$$

Where subscript "c" indicates a continuous phase, ρ, is the liquid density in the bubbly regime, but the vapor density in the mist regime. The drag coefficient C_{lv}^{D} can be computed by various models [16].

2- 11- 4- Interfacial lift force

The interfacial lift force has the general form:

$$F_l^L = -F_v^L = -C_{lv}^L \alpha_d \rho_c (V_l - V_v) \times (\nabla \times V_c) \tag{23}$$

Where α_d is the volume fraction of a dispersed phase. V_c is the velocity vector of a continuous phase. The coefficient, C_{lv}^L can be calculated by Moraga et al. or Tomiyama et al. formulations [23] in bubbly flow regimes, while it is assumed to be zero in droplet flows.

2- 11- 5- Turbulent drift force

In the RPI boiling model, the turbulent drift force is computed as [24]:

$$F_{lv}^{TD} = -F_{vl}^{TD} = -C_{TD} \rho_c \, ke_c \, \nabla \alpha_d \tag{24}$$

Here ke_c is the turbulent kinetic energy of the continuous phase. The turbulent disperse coefficient C_{TD}, by default, is set to 1.

2- 12- Modified RPI wall boiling model

In order to model the critical heat flux phenomenon, it is crucial to include the vapor temperature variation in the governing equations, while in the conventional RPI model, the vapor temperature is not calculated by solving the phase energy equation but is fixed at the saturation temperature. In addition, thin liquid films along heated walls also need to be taken into account in the wall heat flux partitioning equation. For that reason, the wall heat partition is modified as follows [22]:

$$\dot{q}_w = (\dot{q}_c + \dot{q}_Q + \dot{q}_E + \dot{q}_F) f(\alpha_l) + (1 - f(\alpha_l)) \dot{q}_v + \dot{q}_G \tag{25}$$

The function $f(\alpha_v)$ is in terms of the local vapor volume. It can be predicted by the relation offered by Ioilev et al. [23, 24]:

$$f(\alpha_v) = 1 - f(\alpha_l) = \max\left(0, \min\left\{1, \frac{\alpha_v - \alpha_{v,1}}{\alpha_{v,2} - \alpha_{v,1}}\right\}\right) \tag{26}$$

3- Submission of Papers to Journal

This section presents some results which include the modeling of single-phase flow field in the normal conditions in order to investigate the mixing vanes operation and adjusting the available code. In the next step, the effectiveness of mixing vane installation under accident conditions in a boiling flow field accompanied by dryout phenomenon has been examined eventually.

3- 1- Single and two-phase flow boiling

The first validation case is a 3D PWR core channel as shown in Fig. 2. In this figure, a schematic of the 5×5 fuel rod bundle and mixing vane geometry attached to the spacer grid with an angle of 25 degrees accompanied by its arrangement have been illustrated. For further detailed information, one could refer to reference [4, 25]. The inlet boundary conditions considered in the present simulation correspond to the experiments performed by Karoutas et al. [25], with temperature and operating pressure set to 26.67 °C and 4.83 bar, respectively. An axial inlet velocity equal to 6.79 m/s was defined at the entrance of the bundle.

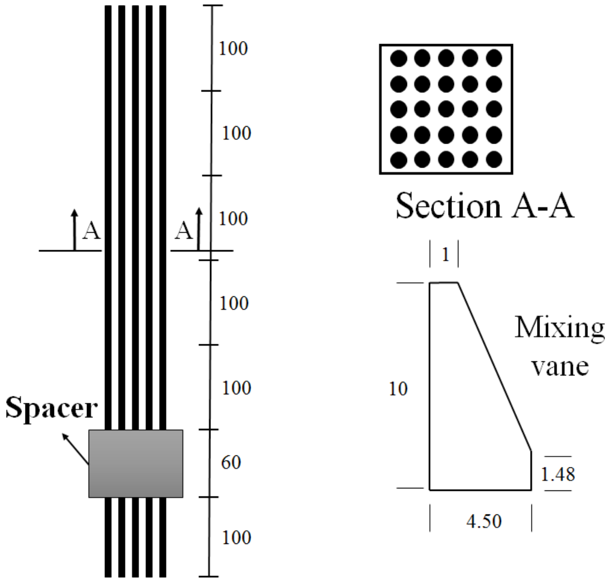

Fig. 2. Schematic of PWR core channel and the employed mixing vane geometry (dimensions in mm)

Figs. 3 and 4 depict the computational model with the associated grids and a schematic of the extended region of the mixing vanes attached to the spacer grids. It is noted that due to the imposed symmetric boundary condition, the extended computational domain could be developed as shown in the left-hand side of the Fig. 4. In order to investigate the grid independency of the solution, unstructured grids with 923169 and 1296116 cells, were employed and the two grids returned almost similar solutions.

Figs. 5 and 6 present a comparison between the computations and the experimental data consisting of static pressure along the channel and lateral velocity at section 0.1905 meters from the inlet. As can be seen from these figures, the results of the current study along with the Karatous and In et al. computations [25, 26] are in a close agreement with the experimental data.

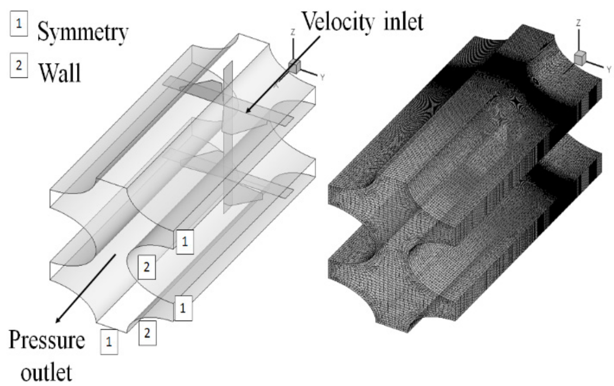

Fig. 3. Schematic of the computational domain and the associated mesh topology

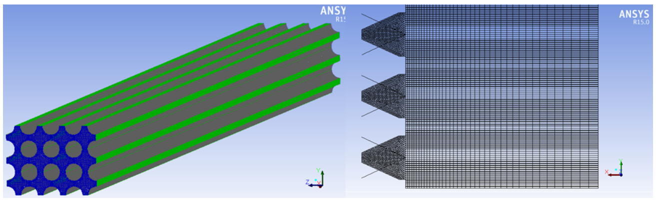

Fig. 4. An extended view of the computational domain (left) and mixing vanes attached to the spacer grid (right)

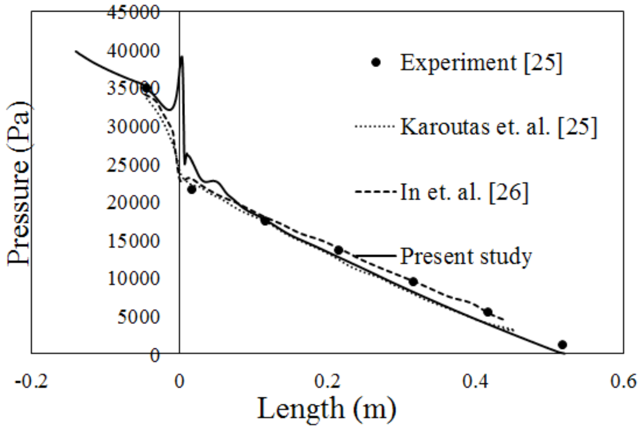

Fig. 5. Pressure distribution along the channel

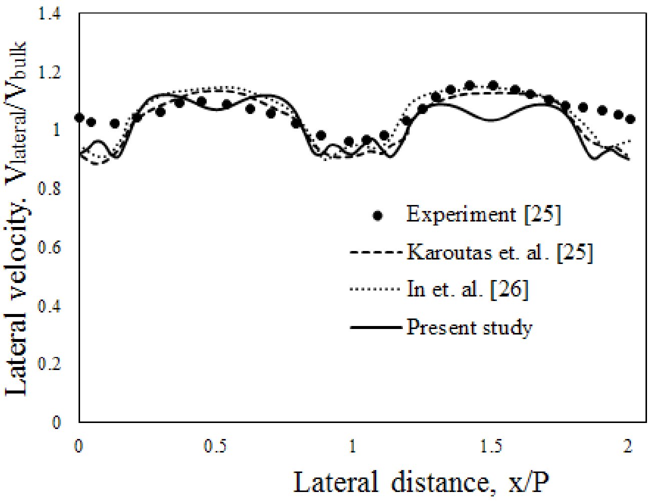

Fig. 6. Velocity distribution versus the dimensionless lateral distance based on pitch (*P*) at 0.1905 meters from the entrance region

As an introduction to approach the critical heat flux phenomenon, the boiling case of the current study by applying a heat flux equal to 5000 kW/m^2 has been investigated. Fig. 7 represents the boiling heat transfer coefficient. As can be seen from this figure, the presence of the spacer grid has led to a sharp increase in the local heat transfer coefficient.

3- 2- Critical heat flux results

In the current section, the results of the critical heat flux phenomenon due to the excessive heat are reported in a vertical rod bundle. It is notable that the effects of mixing vanes are discussed subsequently. Experiments were performed in the THTF (Thermal-Hydraulic Test Facility), carried out by the ORNL (Oak Ridge National Laboratory)

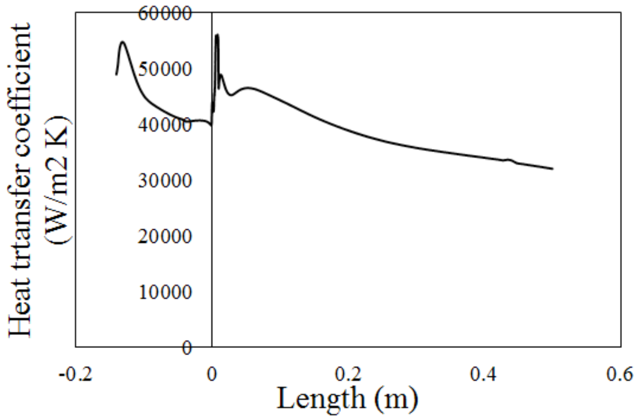

Fig. 7. Boiling heat transfer coefficient along the channel

[27]. THTF is nonnuclear pressurized water loop containing 64 full-length rods (fuel rod simulator) arranged in an 8 × 8 bundle. Rod diameter (0.0095 m) and pitch (0.0127 m) are typical of a PWR with 17 × 17 fuel assemblies (Fig. 8). The axial and radial power distributions of the THTF bundle are flat. The heated length and diameter of the bundle are 3.66 m and 0.95 cm, respectively. There are six spacer grids in the heated length. At the inlet, water enters the channels with subcooling temperature equal to 19.1 K, the saturation temperature of 602.56 K and the wall heat flux on the heated rods is 0.914 MW/m^2. Liquid flows upward through the subchannels with a mass flux of 705 kg/m^2 s under operating pressure of 12.76 MPa. Figs. 9 and 10 depict a schematic of the corresponding channel with boundary conditions and the associated computational grids, respectively.

It is observed that the amount of 823310, 835820 and 835820 computational cells for the cases accompanied by mixing vane of 0, 15 and 25 degrees have been used, respectively.

Fig. 11 represents the wall temperature distribution with and without the spacer grids besides experimental data [27] together with Jun et al. [7]. It can be seen that a jump in the wall temperature with an average magnitude approximately equal to 1000 K has occurred in the vicinity of 1.6 m from the inlet according to experimental data. As can be observed, the temperature profiles are in a relatively good agreement

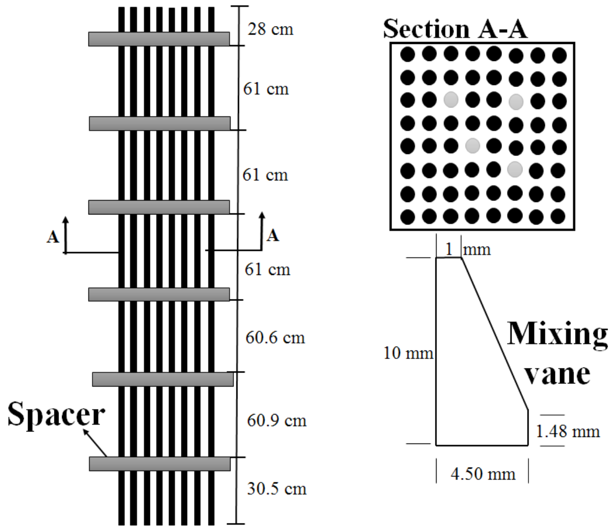

Fig. 8. Schematic of PWR core channel and the employed mixing vane geometry (dimensions in mm)

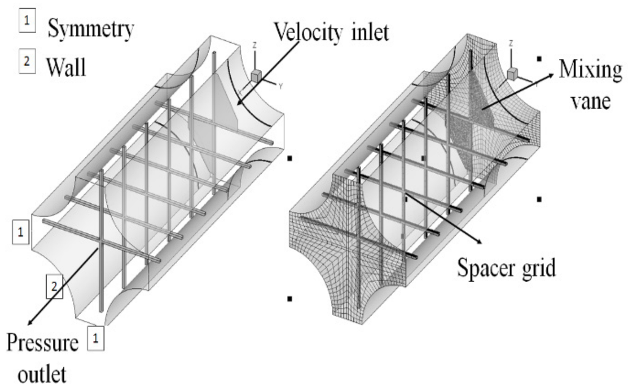

Fig. 9. A schematic of the geometry and the employed mesh

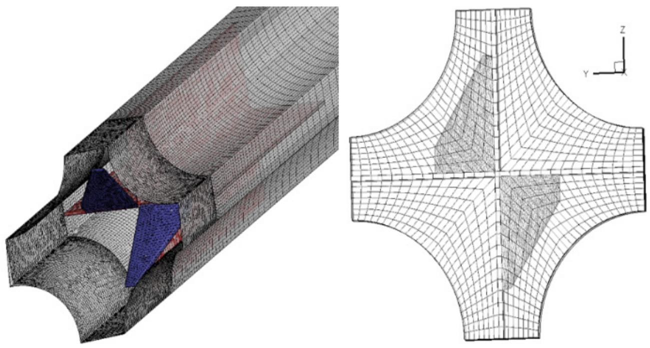

Fig. 10. Representation of the grids employed to model the computational domain

with the experiment and a better solution has been achieved compared to the Jun et al.'s result, although the current study predicts the temperature jump location earlier. It is noteworthy to say that the presence of the spacer grids predicts the temperature jump location better compared to the experimental data; however, it slightly underestimates wall temperature in the post-CHF region except for the near exit region which is in a good agreement with the test data. It is also evident that in the case of the spacer grids, there exist some fluctuations in the wall temperature as a result of the spacer grids presence particularly after the occurrence of the temperature jump.

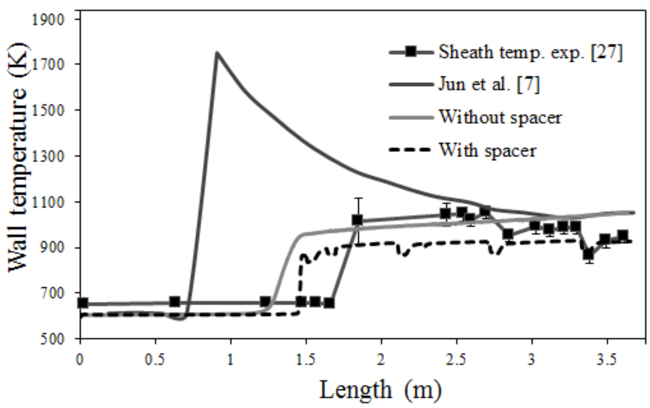

Fig. 11. Wall temperature distribution along the channel

3- 2- 1- CHF and post-dryout in rod bundle in the presence of mixing vanes

As illustrated in the preceding section, post-CHF heat transfer regimes are inefficient and its occurrence can cause a large temperature gradient in the heated wall, leading to physical burnout. In this section, it is tried to enhance the critical heat flux threshold by adding mixing vanes to different angles. It is noteworthy to mention that the geometric configuration and boundary conditions are the same as previous section 2.2. The problem is treated as a steady-state, liquid-vapor two-phase turbulent boiling flow of water with the saturation temperature of 602.56 K.

The influence of mixing vanes with different angles attached to the spacer grids on thermal-hydraulic properties is represented in Fig. 12. It can be seen that sudden changes in the wall temperature will be delayed in the presence of the mixing vanes with different angles. It is noteworthy to mention that increasing the angle of the mixing vanes from 0 to 25 degrees, postpones the sudden temperature rise and also decreases the maximum temperature value.

Fig. 13 shows the surface Heat Transfer Coefficient (HTC) in the presence of mixing vanes with different angles. It is apparent that HTC gradually decreases in the near entrance region when the liquid layer touches the heated wall. On the other hand, HTC drops suddenly, indicating that burnout phenomenon would occur. It is also obvious that by an increase in the mixing vane angle, the sharp reduction location would be delayed, resulting in a more efficient heat removal from the fuel rods.

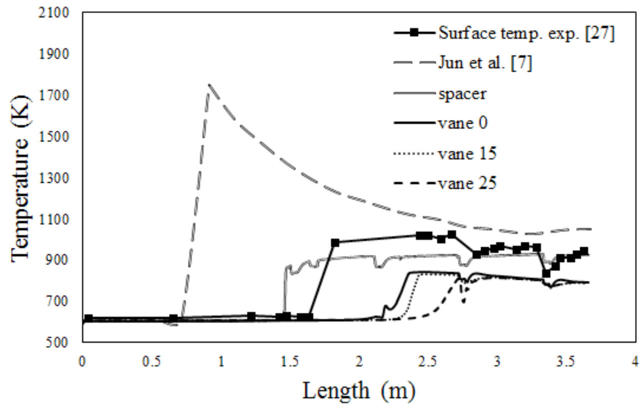

Fig. 12. Wall temperature variation with different vane angles

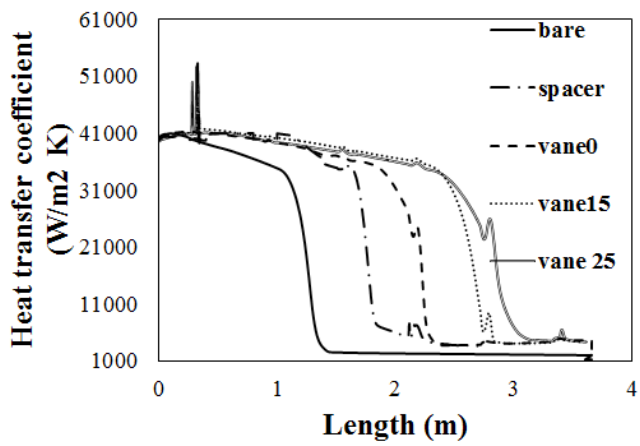

Fig. 13. Surface heat transfer coefficients along the channel

The average heat transfer coefficients for different cases have been computed and gathered in Table 1. As can be seen, the

Table 1. Average heat transfer coefficient (W/m²K)

	Spacer grid	Vane0	Vane15	Vane25
h	19222	25069	26333	27222

presence of vane with an angle of 25 degrees would enhance the heat transfer coefficient to approximately 40 percent.

Description of velocity vectors at a section after the vane with 25 degrees angle has been depicted below in Fig. 14. As can be seen from this figure, the presence of vane leads to the rotational flow after the van and consequently increases the turbulent intensity and heat transfer capacity.

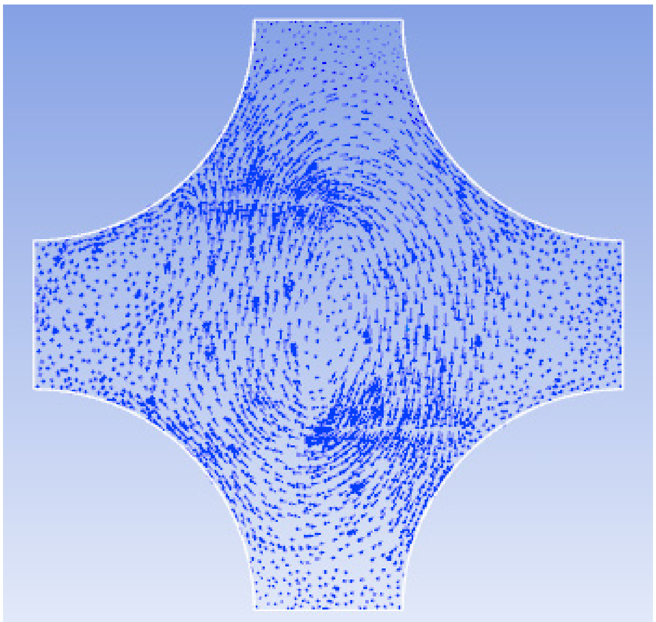

Fig. 14. Illustration of velocity vectors at a section after the vane with 25 degrees angle

Fig. 15 represents the vapor volume fraction along the channel in the presence of the spacer grids with different mixing vane angles. Despite the sudden change in the wall temperature, the vapor volume fraction has increased gradually along the channel. As can be seen, increasing the vane angle reduced the rate of vapor formation particularly in the vicinity of the entrance region.

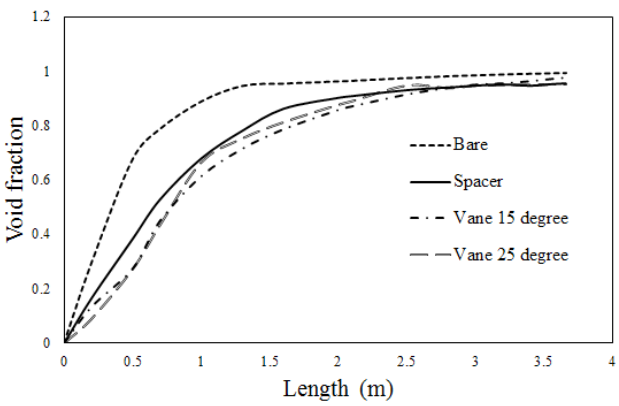

Fig. 15. Area averaged vapor volume fraction in the presence of the spacer and mixing vanes

Fig. 16 depicts the wall heat partitioning for the mixing vane with 25 degrees as a typical case. The sum of the different wall heat flux partitions is equal to the total heat flux (900000 W/m^2). It is evident that up to the length 2.5 m from the channel inlet, almost all of the heat flux applied to the wall is allocated to the evaporation heat flux contribution while at downstream of the post-dryout, vapor heat flux plays a dominant role. It is notable that all of the following results correspond to the mixing vane with 25 degrees.

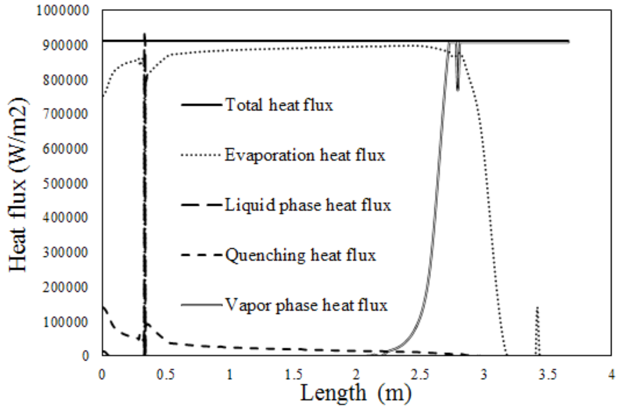

Fig. 16. Heat flux partitioning along the channel for the mixing vane with 25 degrees

Fig. 17 shows the water volume fraction contours at several selected sections along the channel. It could be seen that water begins to evaporate immediately after entering the heated channel and the vapor volume fraction steadily increases along the axial direction.

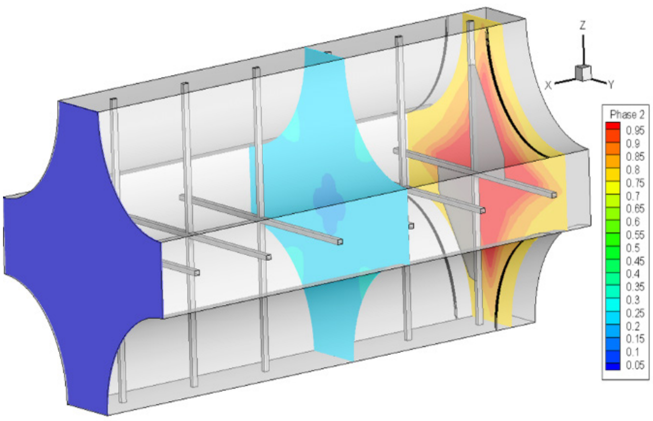

Fig. 17. Water volume fraction at different sections before and after the mixing vane

Water volume fractions at different sections before and after the mixing vane and also for the case without mixing vane have been illustrated in Figs. 18 and 19, respectively. Based on these figures and Fig. 15 in the manuscript, the presence of the vanes due to the enhanced turbulent intensity, the amount of the void fraction along the wall channel has been decreased.

A description of the temperature contours has been depicted in Fig. 20. As can be seen, the near-wall liquid layer has been highly affected by the heated wall in comparison with other regions.

Figs. (21-24) show liquid and vapor velocities at the sections, 0.25, 0.335, 2 and 3.65 meters before and after the occurrence of the dryout along the channel and at the outlet, as well.

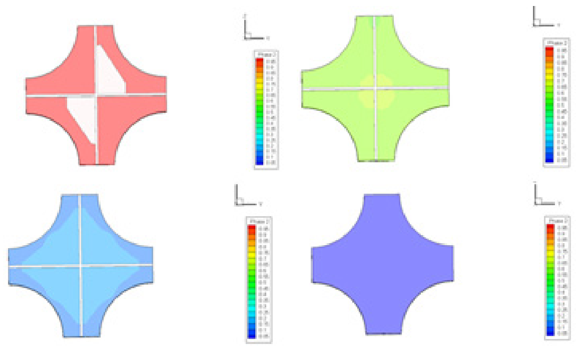

Fig. 18. Water volume fraction contours in the presence of vanes

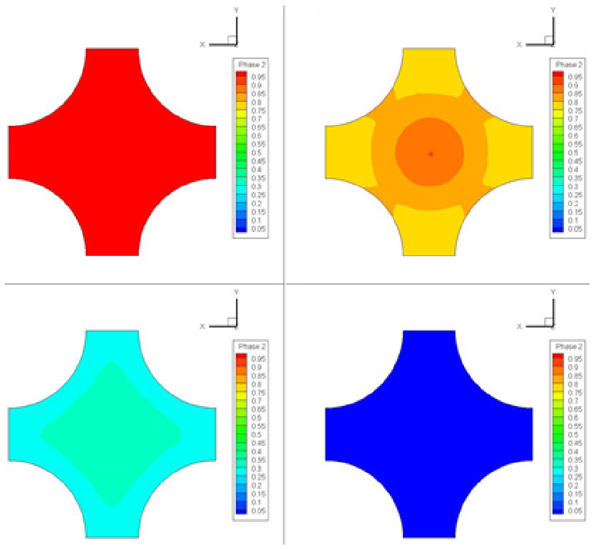

Fig. 19. Water volume fraction contours without vanes

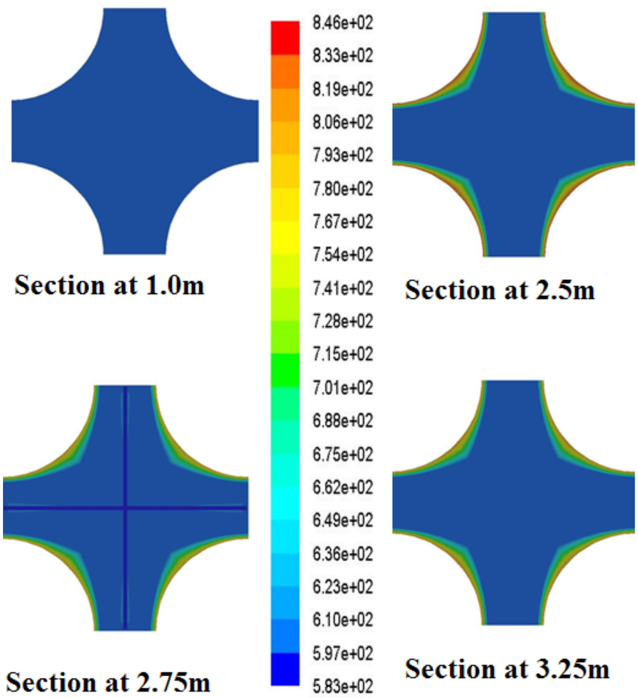

Fig. 20. Liquid temperature distribution at various sections

Due to the departure from nucleate boiling occurrence, it is evident that a significant increase in the speed of the phases has happened. It is also seen that at identical sections, the liquid and vapor velocity distributions are not equal, which suggests that there exists a slip velocity between the two phases. It is notable that due to the swirling flow as a result of the existence of mixing vanes, there is an asymmetry in the lateral velocity profiles, however, as the flow approaches the exit region, this asymmetry would be diminished.

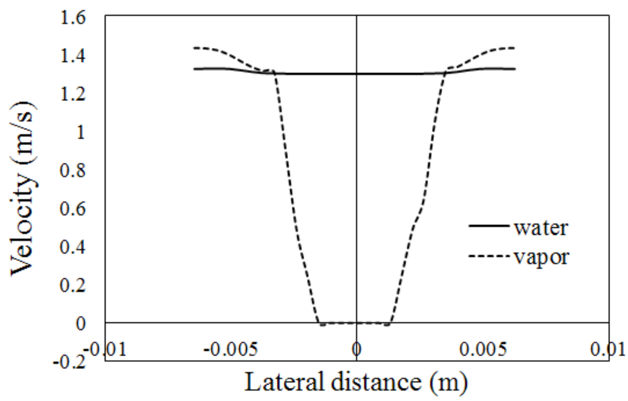

Fig. 21. Lateral velocity of the water and vapor phases at section 0.25 meters from the inlet

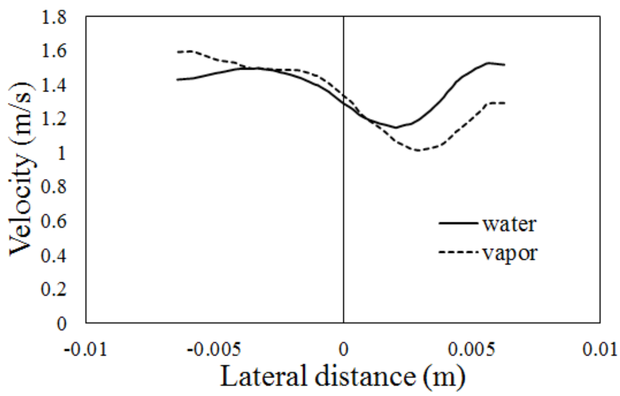

Fig. 22. Lateral velocity of the water and vapor phases at section 0.335 meters from the inlet

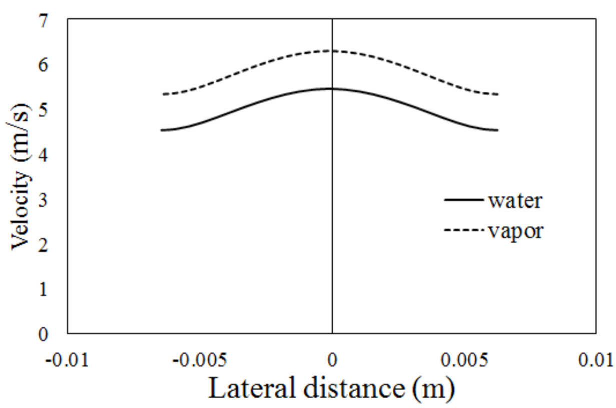

Fig. 23. Lateral velocity of the water and vapor phases at section 2.0 meters from the inlet

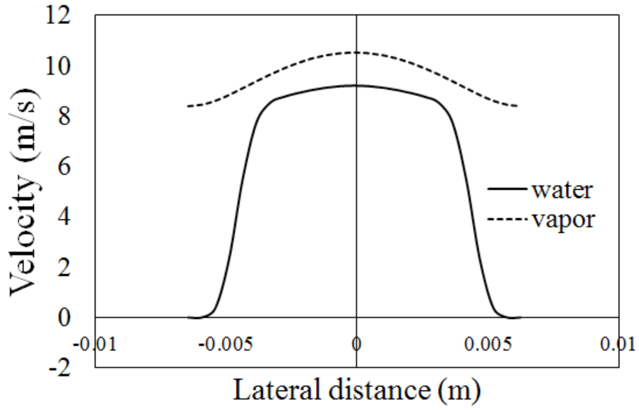

Fig. 24. Lateral velocity of the water and vapor phases at section 3.6 meters from the inlet

4- Conclusion

In this research, efforts have been made to examine the effects of the mixing vanes attached to the spacer grids on the flow field in CHF conditions. In order to simulate the boiling flow field, averaged Navier-Stokes equations have been used with a Eulerian- Eulerian approach for each phase and wall boiling phenomenon is modeled using the mechanistic RPI model and the extended formulations for the departure from nucleate boiling, as well. In the first step, a 5×5 PWR fuel rod bundle was simulated in order to adjust the available code and it was observed that a fairly good agreement was achieved between the results and the experimental data. The main objective of this study was to investigate the critical heat flux phenomenon in an 8×8 rod bundle in the existence of spacer grids accompanied by the mixing vanes with different angles on the deviation from nucleate boiling. According to the obtained results, the presence of the spacer grid alone in the flow field postpones the occurrence of the dryout phenomenon to about 0.25 meters (Fig. 11) and also increasing the vane angle to 25 degrees delays the sudden temperature rise approximately about 1 meter (Fig. 12). In addition, attaching the mixing vanes to the spacer grid also improves the heat transfer characteristics of the flow field such that it delays the sudden temperature jump occurrence and also decreases the maximum temperature value about 100 degrees (Fig. 12). Moreover, it was concluded that increasing the mixing vane angle from 0 to 25 degrees further promotes the heat transfer coefficient of the system about 40 percent based on Table 1. It can be summarized that the presence of mixing vanes in the flow field enhances the heat transfer performance of the system and consequently improves the safety margins leading to a secure operation of the nuclear reactor in both normal and accident conditions.

References

[1] B. S. Shin, S. H. Chang, Experimental study on the effect of angles and positions of mixing vanes on CHF in a 2×2 rod bundle with working fluid R-134a, *nuclear engineering and design*, (235) (2005) 1749-1759.

[2] C. M. Lee, J. Soo,Y. D. Choi, Thermo-Hydraulic Characteristics of Hybrid Mixing Vanes in a 17x17 Nuclear Rod Bundle, *Journal of mechanical science and technology*, (21) (2007) 1263-1270.

[3] E. Krepper, B. Koncar, Y. Egorov, CFD modelling of subcooled boiling—Concept, validation and application to fuel assembly design, *Nuclear engineering and design*, (237) (2007) 716-731.

[4] M. A. Navarro, A. C. Santos, 2009. Evaluation of a numeric procedure for flow simulation of a 5X5 PWR rod bundle with a mixing vane spacer, *International Nuclear Atlantic Conference*, Rio de Janeiro,RJ, Brazil, (2009) September27 to October 2.

[5] B. S. Shin, S. H. Chang, CHF experiment and CFD analysis in a 2×3 rod bundle with mixing vane, *nuclear engineering and design*, (239) (2009) 899-912.

[6] M. Damsohn, H. M. Prasser, Experimental studies of the effect of functional spacers to annular flow in subchannels of a BWR fuel element, *Nuclear engineering and desing*, (240) (2010) 3126-3144.

[7] I. S. Jun, K. H. Bae, Y. J. Chung, Validation of the TASS/SMR-S Code for the Core Heat Transfer Model on the Steady Experimental Conditions. *Journal of energy and power engineering*, (2012) 338-345.

[8] A. W. Bennett, G. F. Hewitt, H. A. Kearsey, et al. Heat transfer to steam-water mixtures flowing in uniformly heated tubes in which the critical heat flux has been exceeded, *Proceedings of the Institution of Mechanical Engineers*, Sept. (1976) 258-267.

[9] S. Jayanti, K. R. Reddy, Effect of spacer grids on CHF in nuclear rod bundles, *Nuclear engineering and desing*, (261) (2013) 66-75.

[10] M. Nazififard, P. SOROUSH, M.R. Nematollahi, Heat Transfer and safety enhancement analysis of fuel assembly an advanced pressurized water reactors: A CFD approach, *Indian J. Sci. Res*, 1(2) (2014) 487-495.

[11] X. Zhu, S. Morooka, Y. Oka, Numerical investigation of grid spacer effect on heat transfer of supercritical water flows in a tight rod bundle, *International journal of thermal sciences*, (76) (2014) 245-257.

[12] H. Seo, S. D. Park, S. B. Seo, H. Heo, I. C. Bang, Swirling performance of flow-driven rotating mixing vane toward critical heat flux enhancement, *International journal of Heat and Mass transfer*, (89) (2015) 1216-1229.

[13] S. Mimouni, C. Baudry, M. Guingo, J. Lavieville, N. Merigoux, N. Mechitoua, Computational multi-fluid dynamics predictions of critical heat flux in boiling flow, *Nuclear engineering and design*, (299) (2015) 59-80.

[14] D. Chen, Y. Xiao, S. Xie, D. Yuan, X. Lang, Z. Yang, Y. Zhong, Q. Lu, Thermal–hydraulic performance of a 5×5 rod bundle with spacer grid in a nuclear reactor, *Applied thermal engineering*, (103) (2016) 1416-1426.

[15] M. Zhao, H. Y. Gu, H. B. Li, X. Cheng, Heat transfer of water flowing upward in vertical annuli with spacers at high pressure conditions, *Annals of nuclear energy*, (87) (2016) 209-216.

[16] H. Li, H. Punekar, S. A. Vasquez, R. Muralikrishnan, Prediction of Boiling and Critical Heat Flux using an Eulerian Multiphase Boiling Model, Proceedings of the ASME, *International Mechanical Engineering Congress & Exposition*, Colorado,USA (2011).

[17] N. Kurul, M. Z. Podowski, On the modeling of multidimensional effects in boiling channels. In: *Proceedings of the 27th National Heat Transfer Conference*, Minneapolis, Minnesota, USA, July (1991).

[18] V. H. D. Vall, D. B. R. Kenning, Subcooled flow boiling at high heat flux, *Int. J. Heat Mass Transfer*, (28) (195) 1907-1920.

[19] R. Cole, A photographic study of pool boiling in the region of the critical heat flux. *AICHE J.* (6) (1960) 533-542.

[20] M. Lemmert, J. M. Chawla, Influence of flow velocity on surface boiling heat transfer coefficient. *Heat Transfer in Boiling*, (1977) 237-247.

[21] V. I. Tolubinski, D. M. Kostanchuk, Vapor bubbles growth rate and heat transfer intensity at subcooled water boiling. In: *4th International Heat Transfer Conference*, Paris, France (1970).

[22] H. Li, S. A. Vasquez, H. Punekar, Prediction of Boiling and Critical Heat Flux Using an Eulerian Multiphase Boiling Model. Proceedings of the ASME 2010, *International Mechanical Engineering Congress & Exposition*, canada (2010).

[23] A. Ioilev, M. Samigulin, V. Ustinenko, Advances in the modeling of cladding heat transfer and critical heat flux in boiling water reactor fuel assembly, *NURETH-12*, Pittsburgh, Pennsylvania, USA (2007).

[24] A. A. Troshko, Y. A. Hassan, A two-equation turbulence model of turbulent bubbly flow, *Int. J. Multiphase Flow*, 22(11) (1965) 2000-2001.

[25] Z. Karoutas, C. Gu, B. Sholin, 3-D flow analyses for design of nuclear fuel spacer. In: *Proceedings of the 7th International Meeting on Nuclear Reactor Thermal-hydraulics NURETH-7*, New York, USA, 3153e3174 (1995).

[26] W. K. In, D. S. Oh, T. H. Chun, CFD Analysis of Turbulent Flow in Nuclear Fuel Bundle with Flow Mixing Device, KAERI report, *TR-1296/99*, (1999) 54.

[27] C. B. Mullins, D. K. Felde, A. G. Sutton, S. S. Gould, D. G. Morris, J. J. Robinson, ORNL Rod-Bundle Heat-Transfer Test Data, Vol. 3, Thermal-hydraulic test facility experimental data report for test 3.06.6B-transient film boiling in upflow, *technical report* (1982).

Please cite this article using:

A. Rabiee, L. Moradi, A. Atf, Numerical Analysis of Critical Heat Flux Phenomenon in a Nuclear Power Plant Core Channel in the Presence of Mixing Vanes, *AUT J. Mech. Eng.*, 1(2) (2017) 119-130.

DOI: 10.22060/mej.2017.12928.5472